

Superpixel-Based Line Operator for Retinal Blood Vessel Segmentation

Tong Na^{1,2}, Yitian Zhao^{2(✉)}, Yifan Zhao³, and Yue Liu²

¹ Georgetown Preparatory School, North Bethesda 20852, USA

² Beijing Engineering Research Center of Mixed Reality and Advanced Display,
School of Optoelectronics, Beijing Institute of Technology, Beijing, China
yitian.zhao@bit.edu.cn

³ EPSRC Centre for Innovative Manufacturing in Through-life Engineering Services,
Cranfield University, Cranfield, UK

Abstract. Automated detection of retinal blood vessels plays an important role in advancing the understanding of the mechanism, diagnosis and treatment of cardiovascular disease and many systemic diseases. Here, we propose a new framework for precisely segmenting vasculatures. The proposed framework consists of two steps. Inspired by the Retinex theory, a non-local total variation model is introduced to address the challenges posed by intensity inhomogeneities and relatively poor contrast. For better generalizability and segmentation performance, a superpixel based line operator is proposed as to distinguish between lines and the edges, and thus allows more tolerance in the position of the respective contours. The results on three public datasets show superior performance to its competitors, implying its potential for wider applications.

Keywords: Vessel · Segmentation · Total variation · Retinex · Superpixel · Line operator

1 Introduction

The accurate detection of retinal vessels is essential for many clinical applications to support early detection, diagnosis and optimal treatment. Manual annotation of vascular structure is an exhausting task for graders, and computer-aided automatic/semi automatic vascular detection methods can significantly reduce the amount of time. However, many factors cause inaccuracy in vessel segmentation, including poor contrast, noise and pathologies such as micro-aneurysms, hemorrhages, and exudate.

Over the past two decades, a tremendous amount of vessel segmentation methods have been developed for different types of medical images. Numerous fully automated, semi-automated methods have been proposed, as evidenced by extensive reviews [1–3]. In general, all established automated segmentation methods may be categorized as either supervised segmentation [4–9] or unsupervised segmentation [3, 10–15] regarding the overall system design and architecture.

Unsupervised segmentation refers to methods that achieve the segmentation of blood vessels without using training data or explicitly using any supervised classification techniques [16]. This category includes most segmentation techniques in the literature, such as active contour models [13, 22], wavelets [14], line operator [10] and our new framework, as described in this paper. In contrast, supervised methods [4–8, 17, 28] require a manually annotated set of training images for classifying a pixel either as vessel or non-vessel. Most of these methods in supervised category use Support Vector Machine, AdaBoost, Neural Networks, Conditional Random Field, etc.

However, the computer-aided vessel segmentation have yet to completely solve the challenging problems, such as posed by the high degree of anatomical variation across the population, and to the increasing complexity of the surrounding tissue and varying scales of vessels within an image. Moreover, artifacts during image acquisition, such as noise, poor contrast and low resolution, exacerbate this problem.

In this paper, we proposed a novel vessel segmentation framework. It comprises two main phases: a non-local total variation regularized intensity inhomogeneity correction, and superpixel based line operator segmentation model. The contributions of this work may be summarized as three folds: **(1)** A Retinex-based inhomogeneity correction method is introduced to normalize the imbalance illumination. When it is extended to vessel image intensity inhomogeneity correction, it has showed good performance and facilitates the subsequent processes. **(2)** The sensitivity for the detection of vessels is significantly improved after the superpixel adapted to the line operator. **(3)** The proposed segmentation framework achieves the best performance in the comparison studies on three publically available datasets.

2 Method

In this section, we describe the proposed method for the extraction of vessels by using Retinex-based inhomogeneity correction and superpixel enabled line operator segmentation. The main steps of our approach are illustrated in Fig. 1.

2.1 Retinex-Based Inhomogeneity Correction

The retinal images acquired with a fundus camera sometimes have poor contrast due to too strong or too low illumination conditions, it usually inherited from image acquisition. To this end, an inhomogeneity correction method is proposed to handle these problems in this paper.

The Retinex theory has been successfully adopted to computer vision field [18], in order to remove unfavorable illumination effects from images to improve their quality and contrast. The Retinex theory shows that any given image \mathbf{I} can be modeled as a component-wise multiplication of two components, the reflectance \mathbf{R} and the illumination \mathbf{L} : $\mathbf{I} = \mathbf{L} * \mathbf{R}$. Typically, \mathbf{R} reveals the reflectance of the object of interest more objectively, and can thus be regarded

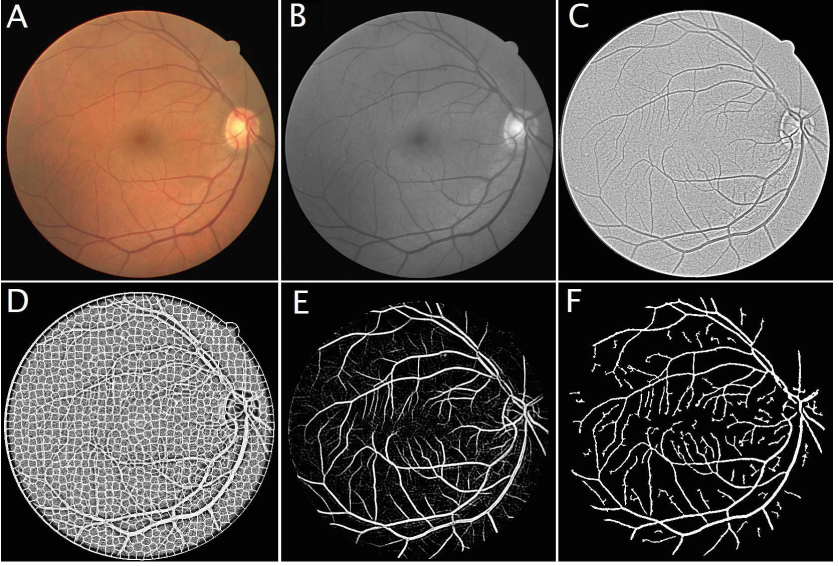


Fig. 1. Overview of the main steps of our method: (A) A random selected color fundus image; (B) The green channel of (A); (C) Results after applying Retinex on (B); (D) Superspixelized results of (C); (E) Vessel response of the proposed method; (F) Segmentation result by the proposed method.

as the enhanced image \mathbf{I} . A look-up-table log operation can transfer this multiplication into an addition, resulting in $i = \log(\mathbf{I}) = \log(\mathbf{L}) + \log(\mathbf{R}) = l + r$ [18]. Clearly, the recovery of l or r is an ill-posed inverse image decomposition problem.

In this paper, a non-local total variation (TV) regularized model supporting the Retinex theory is adopted. It is very effective that the TV regularizer in recovering edges of images [19]. Such phenomenon coincides with the partial differential equation based Retinex method: the reflectance corresponds to the sharp details in the image and the illumination is spatially smooth. The non-local TV regularized model can be formulated as an energy minimization problem as:

$$\mathbf{R} = \arg \min_l \left\{ t \int_{\Omega} |\nabla_w l| + \frac{1}{2} |\nabla(l - i)|_2^2 \right\}, \quad (1)$$

where $l \leq i$. Here, $\int_{\Omega} |\nabla_w l|$ indicates the regularization term, and it is able to find the sharp details. $|\nabla(l - i)|_2^2$ is L_2 term of the gradient of the illumination, it ensures to smooth the illumination. t is the parameter to balance two terms. Ω is the support of the image. For a given image, the non-local weight between pixel \mathbf{x} and \mathbf{y} can be defined as

$$w(\mathbf{x}, \mathbf{y}) = \exp \left\{ \frac{-K * (l(\mathbf{x}) - l(\mathbf{y}))^2}{2h^2} \right\}, \quad (2)$$



Fig. 2. Illustrative results of image enhancement by using non-local total variation based Retinex approach. (A) and (C): The green channel of two random selected color fundus image. (B) and (D): Results after applying Retinex on (A) and (C).

where K is the Gaussian kernel, and h is the control parameter. The non-local gradient operator at pixel \mathbf{x} can be defined by the yielded non-local weights, as the vector of all partial difference $\nabla_w l(\mathbf{x}, \cdot)$:

$$\nabla_w l(\mathbf{x}, \mathbf{y}) = (l(\mathbf{y}) - l(\mathbf{x}))\sqrt{w(\mathbf{x}, \mathbf{y})}, \forall \mathbf{y} \in \Omega. \quad (3)$$

Hence, the non-local TV regularizer can be defined as

$$\int_{\Omega} |\nabla_w l| = \int_{\Omega} \left(\int_{\Omega} (l(\mathbf{y}) - l(\mathbf{x}))^2 w(\mathbf{x}, \mathbf{y}) d\mathbf{y} \right)^{\frac{1}{2}} d\mathbf{x}. \quad (4)$$

Figure 2 shows two enhanced results produced by applying the non-local TV based Retinex model. It has successfully corrected the contrast between vessels and background well, as well as the region of optic disc. In consequence, the vessels are more easily identifiable.

2.2 Superpixel-Based Line Operator

The basic line operator considers 12 angles, and the angular resolution is 15 degree. The largest average grey level \mathbf{L} is found, which the pixel lies on a line passing through the target pixel. Then the line strength of the pixel is defined as

$$\mathbf{S}(i) = \mathbf{L}(i) - \mathbf{N}(i), \quad (5)$$

where $\mathbf{N}(i)$, is the average grey-level of a square window, centered on the target pixel i , with edge length equal to μ . The winning line is aligned within a vessel if the line strength is large, while the line strength is lower if the line is partially overlapped. In general, the length μ is empirically chosen, such as 15 in [10], and 5 in [20].

However, it usually has varying scales of vessels within an image, and a single value of μ always yield imbalance responses on the vessels. Therefore, in order to achieve better segmentation performance, in this work we applied a modified line operator on the superpixel generated patches rather than on entire image, in particular in regions with low signal noise ratio. The length μ was set to be half of the minimum object length of corresponding superpixel.

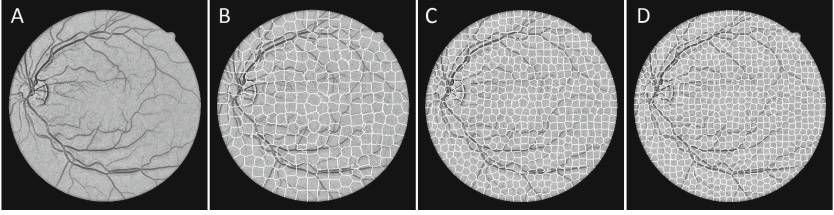


Fig. 3. Illustration of different superpixel numbers generated on an example image: (A) The green channel of a random selected color fundus image; (B) 400 superpixels; (C) 800 superpixels; (D) 1200 superpixels.

To achieve this, we first generate the superpixel upon the vesseliness map. The SLIC superpixel algorithm [21] is adapted to replace the rigid structure of the pixel grid. The SLIC is a k-means clustering based method, and is able to assign each pixel to a superpixel according to their intensities and spatial locations. The superpixel clustering procedure starts with the generation of initial cluster centers. Then a distance measure D to cluster centers for all pixels is defined, aims to associate to their nearest cluster centers. The Euclidean distance (d_c) and spatial distance (d_s) are used to define this measure:

$$D = \sqrt{d_c^2 + \left(\frac{d_s}{S}\right)^2 m^2}, \quad (6)$$

where $S = \sqrt{N/k}$ is the grid interval. k is the desired superpixel number and N is the total number of pixels. m indicates a parameter to balance the weighting of intensity and coordinates. Figure 3 shows an example of superpixel representation, with 400, 800, and 1200 superpixels, respectively.

Let $\mathcal{P}_t \in T$ be a viable local representation as a superpixel t ($t = 1, 2, \dots, T$), and let I indicate the input image. The line strength of the pixel in superpixel \mathcal{P} is defined as $\mathbf{S}_{\mathcal{P}_t}(i) = \mathbf{L}_{\mathcal{P}_t}(i) - \mathbf{N}_{\mathcal{P}_t}(i)$. In practice, the line path is hard to be exactly matched the pixel grid, hereby, the line and region averages at arbitrary orientations are obtained by using nearest neighbour interpolation instead of bi-linear interpolation.

Multiscale analysis is also performed in this framework. The line strength of the pixel under multi-level superpixel is defined as

$$\mathbf{S}(i) = \frac{1}{P} \sum_{p=1}^P \mathbf{S}(i)(\mathcal{P}_t^p | i \in \mathcal{P}_t^p). \quad (7)$$

where P indicates the levels of superpixels that the input image is segmented to. Parameter tuning for optimal numbers of superpixels and levels (P and M) will be discussed in Sect. 4.2. The second column of Fig. 4 demonstrate the final vessel responses of the proposed method. In order to extract the vessel from the response map, our previous proposed infinite perimeter active contour with hybrid region (IPACHR) method [23] is employed for its good performance. The

IPACHR uses an infinite perimeter active contour model for its effectiveness in detecting vessels with irregular and oscillatory boundaries. For more details, we refer readers to the original paper [23]. The third column of Fig. 4 depict the segmentation results.

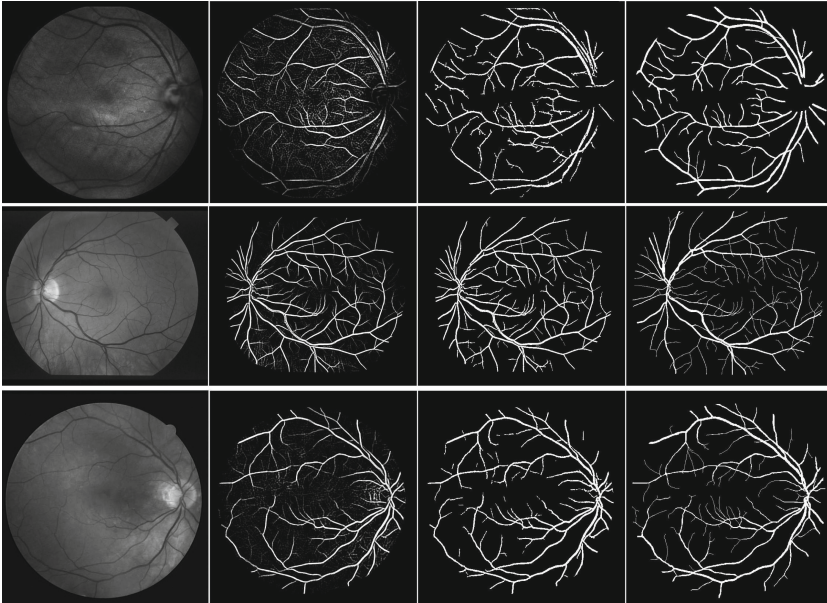


Fig. 4. Examples of vessel segmentation by the proposed method on 3 datasets. From left to right: green channel of random selected color fundus images, results after super-pixel enabled line operator, automated segmentation results, and manual annotations.

3 Datasets and Evaluation Metrics

Three publically available retinal datasets are used in this work to evaluate the proposed segmentation framework: STARE¹, DRIVE², and a newly released dataset IOSTAR³. The image resolutions of these datasets are 565×584 , 700×605 , and 1024×1024 , respectively.

The segmentation performance is measured by sensitivity se , specificity sp , and accuracy acc . They are defined as $se = \frac{tp}{tp+fn}$, $sp = \frac{tn}{fp+tn}$, $acc = \frac{tp+tn}{tp+fp+tn+fn}$, respectively. Here, true positive tp is the count of pixels marked as vessel pixels in both the segmented image and its ground truth. Similarly,

¹ <http://www.ces.clemson.edu/~ahoover/stare/>.

² <http://www.isi.uu.nl/Research/Databases/DRIVE/>.

³ <http://www.retinacheck.org>.

false positive fp identifies the number of incorrectly identified vessel pixels; true negative tn is the number of correctly identified non-vessel pixels; false negative fn indicates the number of incorrectly identified non-vessel pixels. In general, reporting the se and sp obtained at highest acc is a common way in the retinal image segmentation. However, it is possible to produce imbalanced results where a higher sp is favored since vessel has relatively lower amount than background. In such a case, acc will be skewed by the dominant classes. Consequently, in order to evaluate the performance of the proposed vessel segmentation method, the receiving operator characteristics (ROC) curve is computed with true positive ratio versus the false positive ratio. The area under the ROC curve (AUC) is calculated to quantify the performance of the segmentation, since it has the ability to reflect the trade-offs between the sensitivity and specificity.

4 Experimental Results

In this experiment, the green channel of the color fundus images were used for vessel segmentation. Figure 4 illustrates examples of vessel detection performance on three datasets, and manual annotation from observer 2 of the DRIVE and STARE dataset were used as groundtruth.

To reveal the relative performance of our proposed method, we compared it with several existing state-of-the-art vessel detection methods on the most popular datasets: DRIVE and STARE. The results are shown in Table 1, and the chosen methods have been ordered by the category the methods belonging to: the most recent seven supervised methods [4–8, 17, 28], and nine unsupervised segmentation methods [3, 10, 14, 15, 23–27]. Overall, our framework yields state-of-the-art performance and outperforms most methods reported in most of the quality metrics used, as it took into account the global features through the Retinex analysis and the local features through the supervoxel-based line operator, therefore, more fine vessels may be detected. For accurate analysis of the DRIVE dataset, the proposed method yields the highest sensitivity, accuracy, and AUC among unsupervised method, and only the sensitivity is lower than the supervised method proposed by Orlando et al. [17]. Note, to the best knowledge of the authors, only Zhang et al. [27] has tested their segmentation method on IOSTAR dataset. In consequence, we only compared with the performance obtained by [27] in the bottom of Table 1, and is by no means exhaustive. In contrast, our method has better performance in terms of all metrics.

Furthermore, three state-of-the-art vessel enhancement methods were employed for comparison purposes. These methods were: isotropic undecimated wavelet filter [14], local phase filter [29] and Combination Of Shifted Filter Responses (BCOSFIRE) [15]. In the interests of reproducibility, the recommended parameters in the literature were used in the experiments. In Fig. 5, we show examples of applying different enhancement methods on a representative patch with multiple vascular bifurcations, curvature changes, intensity inhomogeneity on large vessel and low intensities on tiny vessels. Overall, the proposed method is not only able to detect the vessel regions, but also has the

Table 1. Performance of different segmentation methods, in terms of sensitivity (se), specificity (sp), accuracy (acc) area under the curve (AUC), on the **DRIVE**, **STARE** datasets, and **IOSTAR**.

Method	DRIVE				STARE			
	se	sp	acc	AUC	se	sp	acc	AUC
Second observer	0.776	0.972	0.947	0.874	0.895	0.938	0.934	0.917
<i>Supervised methods</i>								
Staal [4]	-	-	0.946	0.952	-	-	0.951	0.961
Soares [5]	0.733	0.782	0.946	0.961	0.721	0.975	0.948	0.967
Lupascu [6]	0.720	-	0.959	0.956	-	-	-	-
You [7]	0.741	0.975	0.943	-	0.726	0.975	0.949	-
Marin [8]	0.706	0.980	0.945	0.959	0.694	0.981	0.952	0.977
Li [28]	0.757	0.982	0.953	0.974	0.773	0.984	0.963	0.988
Orlando [17]	0.789	0.968	-	-	0.768	0.974	-	-
<i>Unsupervised methods</i>								
Ricci [10]	-	-	0.963	0.960	-	-	0.968	0.965
Palomera-Perez [24]	0.660	0.961	0.922	-	0.779	0.940	0.924	-
Fraz [3]	0.715	0.976	0.943	-	0.731	0.968	0.944	-
Bankhead [14]	0.703	0.971	0.937	-	0.758	0.950	0.932	-
Zhao [23]	0.742	0.982	0.954	0.862	0.780	0.978	0.956	0.874
Yin [25]	0.725	0.979	0.940	-	0.854	0.942	0.933	-
Roychowdhury [26]	0.740	0.978	0.949	0.967	0.732	0.984	0.956	0.967
Azzopardi [15]	0.766	0.970	0.944	0.961	0.772	0.970	0.950	0.956
Zhang [27]	0.747	0.976	0.947	0.952	0.768	0.976	0.955	0.961
Proposed method	0.768*	0.970	0.954*	0.970*	0.781	0.977	0.957*	0.968*
	IOSTAR							
Zhang [27]	0.755	0.974	0.951	0.962				
Proposed method	0.761	0.975	0.955	0.964				

ability to suppress noise and artifacts. In other words, the results obtained by the proposed method seem more pleasing: stronger enhancement results on tiny vessels, better responses on bifurcations/crossovers, and higher uniformity on intensity inhomogeneity.

4.1 The Effectiveness of Superpixel and Retinex

In this section, the effectiveness of line operator enabled with superpixel and Retinex based image enhancement are validated individually.

Figure 6 demonstrates the segmentation results obtained by the proposed models with and without superpixel enabled. It can be observed from Fig. 6(C) that superpixel contributes significantly to the final performance - more tiny vessels have been detected, and helps to improve the sensitivity of the vessel segmentation. This observation is also confirmed by the ROC curves over three

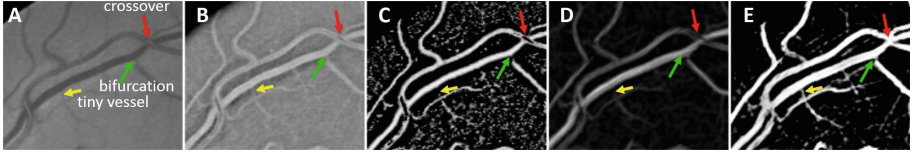


Fig. 5. A comparative study with other enhancement techniques on a selected region with tiny vessel (yellow arrow), bifurcation (green arrow), and crossover (red arrow). (A) The green channel of a selected region of a color fundus image. (B) isotropic undecimated wavelet filter. (C) Local phase. (D) BCOSFIRE. (E) Proposed method. (Color figure online)

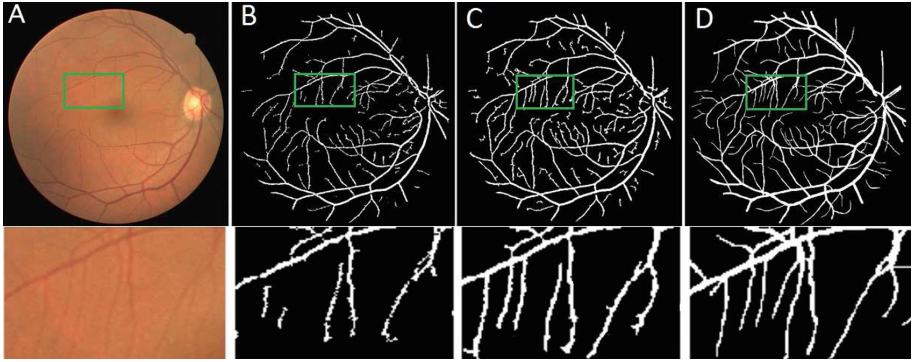


Fig. 6. Segmentation results of the proposed method, and the snapshot of selected region with small vessels. (A) Original image. (B) Segmentation result without superpixel applied. (C) Segmentation result with superpixel applied. (D) Groundtruth. (Color figure online)

different datasets, as illustrated at Fig. 7 (red line). Most existing line operator based segmentation approaches have a certain edge length μ , such as 15 pixels in [10], and 5 pixels in [20]. In this work, the edge length is self-adapting, and it is more sensitive to capture the varying scales of vessels within an image, and this leads to higher *se*, *acc*, and *AUC*.

In addition, the ROC curves of the proposed method with or without Retinex enhancement applied are illustrated at Fig. 7 (green line). Overall, Retinex process affects the final performance significantly, since the optic disk and foveal area always have inhomogeneous intensities, and these inhomogeneities were corrected after Retinex applied. In contrast, the segmentation performances were relative poorer in dataset STARE and IOSTAR than DRIVE when without Retinex applied. That is because STARE and IOSTAR dataset contain some images with pathologies, e.g. presents bright lesions or exudates, blurring vessel, and these features cause more false detections (lower *sp*). While the proposed Retinex method is capable to normalize these regions to a similar level with the background, and increase the contrast between the vessels and background, as thus to avoid the false detection (higher *sp*), and raise the sensitivity score.

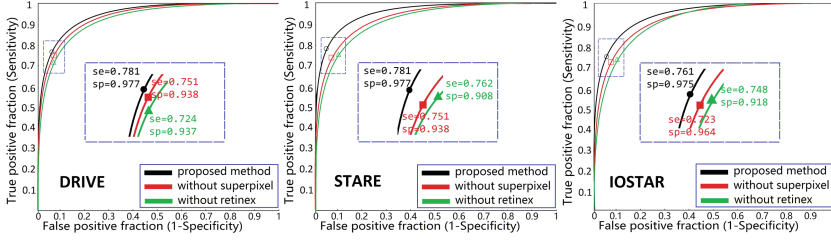


Fig. 7. The ROC curves of the proposed framework with and without the Retinex enhancement applied and superpixel-based the line operator applied over three different datasets respectively. (The reader is referred to the color version of this figure.)

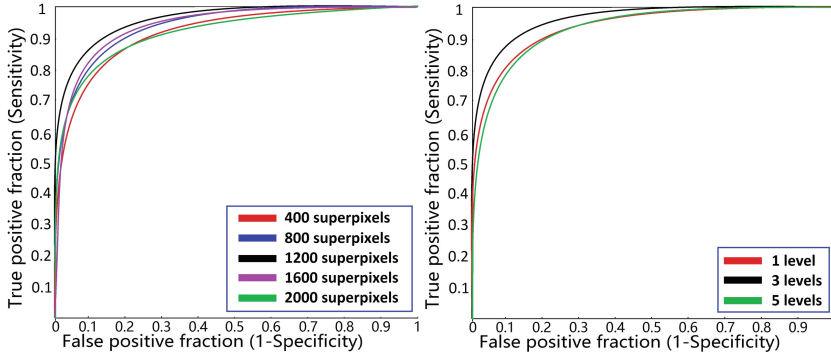


Fig. 8. The ROC curves of the proposed method with (left) different numbers of superpixels: 400, 800, 1200, 1600, and 2000; (right) different numbers of levels, after setting the optimal number of the superpixels to 1200. (The reader is referred to the color version of this figure.)

4.2 Parameters Tuning

In this section, we experimentally investigate the suitable numbers of superpixels M and levels of superpixel partition P . It is known that too large number of superpixel leads to false detection, and on the contrary, too few superpixels result in a loss of the edge information of the vessel [30]. To this end, in this experiment, the numbers of superpixels were set to be successively 400, 800, 1200, 1600, and 2000. The left column of Fig. 8 shows the ROC curve of the proposed method under these numbers, and the proposed method achieves the best result when the superpixel number is 1200. As aforementioned at Sect. 2.2, multiscale analysis was used to detect vessel more precisely when an image contains varying scales of vessels. The right column of Fig. 8 shows the segmentation performance under different superpixel levels when the number of superpixels was set to 1200, and it can clearly be seen that the proposed method yields the best performance when the number of levels is 3. In consequence, the number of superpixels at the other two levels are $\frac{1}{3} \times 1200 = 400$, and $\frac{1}{3} \times 1200 = 800$.

5 Conclusions

In this paper, we have presented a new framework for vessel segmentation, which exploits the advantages of non-local total variation based Retinex model for intensity inhomogeneity correction, and superpixel-based line operator for vessel segmentation. Quantitative evaluations on publically-available datasets showed that, compared to established methods, the proposed method achieves competitive vessel segmentation performance. In particular, it shows better performance in handling small, bifurcation, and crossover vessels, even in the case of poor contrast. It has the potential to become a powerful tool for quantitative analysis of vasculature for the management of a wide range of diseases.

Acknowledgments. This work was supported by National Science Foundation Program of China (61601029, 61602322), China Association for Science and Technology (2016QNRC001), and National Key Research and Development Program of China (2016YFB0401202).

References

1. Kirbas, C., Quek, F.: A review of vessel extraction techniques and algorithms. *ACM Comput. Surv.* **36**, 81–121 (2004)
2. Lesagea, D., Funka-Leaa, G.: A review of 3D vessel lumen segmentation techniques: models, features and extraction schemes. *Med. Image Anal.* **13**, 819–845 (2009)
3. Fraz, M.M., Remagnino, P., Hoppe, A., Uyyanonvara, B., Rudnicka, A.R., Owen, C.G., Barman, S.A.: Blood vessel segmentation methodologies in retinal images - a survey. *Comput. Meth. Prog. Bio.* **108**, 407–433 (2012)
4. Staal, J., Abramoff, M.D., Niemeijer, M., Viergever, M.A., van Ginneken, B.: Ridge-based vessel segmentation in color images of the retina. *IEEE Trans. Med. Imaging* **23**, 501–509 (2004)
5. Soares, J., Cree, M.: Retinal vessel segmentation using the 2D Gabor wavelet and supervised classification. *IEEE Trans. Med. Imaging* **25**, 1214–1222 (2006)
6. Lupascu, C.A., Tegolo, D., Trucco, E.: FABC: retinal vessel segmentation using AdaBoost. *IEEE Trans. Inf. Technol. Biomed.* **14**, 1267–1274 (2010)
7. You, X., Peng, Q., Yuan, Y., Cheung, Y., Lei, J.: Segmentation of retinal blood vessels using the radial projection and semi-supervised approach. *Pattern Recogn.* **44**, 2314–2324 (2011)
8. Marin, D., Aquino, A., Gegundez-Arias, M.E., Bravo, J.M.: A new supervised method for blood vessel segmentation in retinal images by using gray-level and moment invariants-based features. *IEEE Trans. Med. Imaging* **30**, 146–158 (2011)
9. Wang, Y., Ji, G., Lin, P., Trucco, E.: Retinal vessel segmentation using multi-wavelet kernels and multiscale hierarchical decomposition. *Pattern Recogn.* **46**, 2117–2133 (2013)
10. Ricci, E., Perfetti, R.: Retinal blood vessel segmentation using line operators and support vector classification. *IEEE Trans. Med. Imaging* **26**, 1357–1365 (2007)
11. Mendonça, A., Campilho, A.C.: Segmentation of retinal blood vessels by combining the detection of centerlines and morphological reconstruction. *IEEE Trans. Med. Imaging* **25**, 1200–1213 (2007)

12. Martinez-Perez, M., Hughes, A., Thom, S.A., Bharath, A.A., Parker, K.H.: Segmentation of blood vessels from red-free and fluorescein retinal images. *Med. Image Anal.* **11**, 47–61 (2007)
13. Al-Diri, B., Hunter, A., Steel, D.: An active contour model for segmenting and measuring retinal vessels. *IEEE Trans. Med. Imaging* **28**, 1488–1497 (2009)
14. Bankhead, P., McGeown, J., Curtis, T.: Fast retinal vessel detection and measurement using wavelets and edge location refinement. *PLoS ONE* **7**, e32435 (2009)
15. Azzopardi, G., Strisciuglio, N., Vento, M., Petkov, N.: Trainable COSFIRE filters for vessel delineation with application to retinal images. *Med. Image Anal.* **19**, 46–57 (2015)
16. Lathen, G., Jonasson, J., Borga, M.: Blood vessel segmentation using multi-scale quadrature filtering. *Pattern Recogn. Lett.* **31**, 762–767 (2010)
17. Orlandp, J., Prokofyeva, E., Blaschko, M.: A discriminatively trained fully connected conditional random field model for blood vessel segmentation in fundus images. *IEEE Trans. Biomed. Eng.* **64**, 16–27 (2017)
18. Elad, M.: Retinex by two bilateral filters. *Scale Space PDE Methods Comput. Vis.* **3459**, 217–229 (2005)
19. Ng, M.K., Wang, W.: A total variation model for retinex. *SIAM J. Imaging Sci.* **4**, 345–365 (2011)
20. Zwiggelaar, R., Astley, S., Boggis, C., Taylor, C.: Linear structures in mammographic images: detection and classification. *IEEE Trans. Med. Imaging* **23**, 1077–1086 (2004)
21. Achanta, R., Shaji, A., Smith, K., Lucchi, A., Fua, P.: Slic superpixels compared to state-of-the-art superpixel methods. *IEEE Trans. Pattern Anal. Mach. Intell.* **34**, 2274–2282 (2012)
22. Zhao, Y., Zhao, J., Yang, J., Liu, Y., Zhao, Y., Zheng, Y., Xia, L., Wang, Y.: Saliency driven vasculature segmentation with infinite perimeter active contour model. *Neurocomputing* (2017). <http://dx.doi.org/10.1016/j.neucom.2016.07.077>
23. Zhao, Y., Rada, L., Chen, K., Zheng, Y.: Automated vessel segmentation using infinite perimeter active contour model with hybrid region information with application to retinal images. *IEEE Trans. Med. Imaging* **34**, 1797–1807 (2015)
24. Palomera-Prez, M., Martinez-Perez, M., Bentez-Prez, H., Ortega-Arjona, J.L.: Parallel multiscale feature extraction and region growing: application in retinal blood vessel detection. *IEEE Trans. Inf. Technol. Biomed.* **14**, 500–506 (2010)
25. Yin, Y., Adel, M., Bourennane, S.: Retinal vessel segmentation using a probabilistic tracking method. *Pattern Recogn.* **45**, 1235–1244 (2012)
26. Roychowdhury, S., Koozekanani, D., Parhi, K.: Iterative vessel segmentation of fundus images. *IEEE Trans. Biomed. Eng.* **62**(7), 1738–1749 (2015)
27. Zhang, J., Dashtbozorg, B., Bekkers, E., Pluim, P., Duits, B., Romeny, R.: Robust retinal vessel segmentation via locally adaptive derivative frames in orientation scores. *IEEE Trans. Med. Imaging* **35**(12), 2631–2644 (2016)
28. Li, Q., Feng, B., Xie, L., Liang, P., Zhang, H., Wang, T.: A crossmodality learning approach for vessel segmentation in retinal images. *IEEE Trans. Med. Imaging* **35**(1), 109–118 (2016)
29. Zhao, Y., Liu, Y., Zheng, Y.: Retinal vessel segmentation: an efficient graph cut approach with retinex and local phase. *PLoS ONE* **10**, e0122332 (2015)
30. Zhao, Y., Zheng, Y., Liu, Y., Yang, J., Zhao, Y., Chen, D., Wang, Y.: Intensity and compactness enabled saliency estimation for leakage detection in diabetic and malarial retinopathy. *IEEE Trans. Med. Imaging* **36**, 51–63 (2017)

Medical Image Understanding and Analysis

21st Annual Conference, MIUA 2017, Edinburgh, UK, July

11-13, 2017, Proceedings

Valdés Hernández, M.d.C.; González-Castro, V. (Eds.)

2017, XIX, 950 p. 421 illus., Softcover

ISBN: 978-3-319-60963-8